ACS APPLIED MATERIALS & INTERFACES

Research Article

www.acsami.org

# Graphene Oxide–Zinc Oxide Nanocomposite as Channel Layer for Field Effect Transistors: Effect of ZnO Loading on Field Effect Transport

S. Mahaboob Jilani and Pallab Banerji*

Materials Science Centre, Indian Institute of Technology, Kharagpur 721302, India

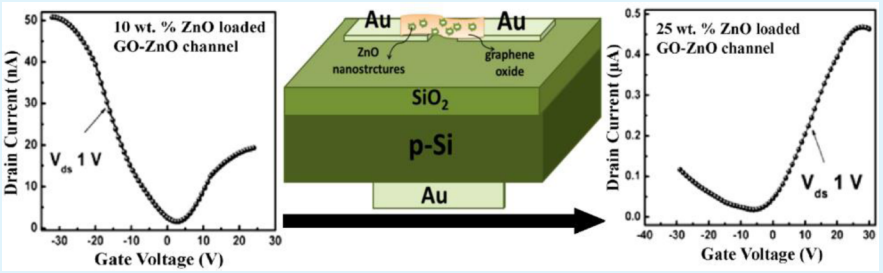


**ABSTRACT:** The effects of ZnO on graphene oxide (GO)–ZnO nanocomposites are investigated to tune the conductivity in GO under field effect regime. Zinc oxides with different concentrations from 5 wt % to 25 wt % are used in a GO matrix to increase the conductivity in the composite. Six sets of field effect transistors with pristine GO and GO–ZnO as the channel layer at varying ZnO concentrations were fabricated. From the transfer characteristics, it is observed that GO exhibited an insulating behavior and the transistors with low ZnO (5 wt %) concentration initially showed *p*-type conductivity that changes to *n*-type with increases in ZnO loading. This *n*-type dominance in conductivity is a consequence of the transfer of electrons from ZnO to the GO matrix. From X-ray photoelectron spectroscopic measurements, it is observed that the progressive reduction in the C–OH oxygen group took place with increases in ZnO loading. Thus, from insulating GO to *p*- and then *n*-type, conductivity in GO could be achieved with reduction in the C–OH oxygen group by photocatalytic reduction of GO with varying degrees of ZnO. The restoration of $sp^2$ electron network in the GO matrix with the anchoring of ZnO nanostructures was observed from Raman spectra. From UV–visible spectra, the band gap in pristine GO was found to be 3.98 eV and reduced to 2.8 eV with increase in ZnO attachment.

**KEYWORDS:** *graphene oxide, zinc oxide, composites, transistors*

## 1. INTRODUCTION

Graphene oxide (GO) has attracted the attention of researchers due to its tunable electrical properties from insulator to graphene like semimetal and its ease of solution processability for large area flexible electronic applications.[1] Graphene oxide is a single layer of graphite (graphene) with oxygen functional groups (carbonyls, hydroxyls, epoxides, etc.) attached on its surface and edges. These functional groups break the $sp^2$ network on the graphene surface and deteriorate its electrical conductivity.[2]

To retain the electrical conductivity in GO, the general practice is to remove the oxygen functional groups by thermal treatment,[3] chemical reduction,[4] hydrogen or ammonia plasma treatment[5] or by photocatalytic reduction using metal oxide nanoparticles.[6,7] Among these methods, the photocatalytic reduction using ZnO nanostructures is attractive for tuning electrical properties as well as to induce *n*-type conductivity in GO. The transistors fabricated using reduced graphene oxide (rGO) as an active layer showed *p*-type electrical conductivity in atmospheric conditions due to adsorption of moisture and oxygen; however, in a vacuum, it is bipolar.[8] To induce *n*-type conductivity, molecules such as potassium[9] or nanoparticles of Au,[10] Pt,[11] or Ce[12] are adsorbed on the rGO surface. Wang et al.[13] reported an *n*-type rGO field effect transistor (FET) by modifying its surface with CdSe or CdS nanocrystals. Yoo et al.[14] showed that by using $TiO_2$ or ZnO nanostructures, *n*-type conductivity could be achieved even in normal atmospheric conditions. In these reports, the GO was first reduced and then the nanocrystals are anchored onto the surface of rGO. Further, the amount (concentration) of nanomaterial loaded is not clearly available in those reports.

In our earlier work,[15] we have reported that *n*-type conductivity could be achieved in GO by embedding ZnO nanostructures (ZnO 25 wt % in GO–ZnO) into a GO matrix where GO was reduced using a photocatalytic reaction. In the present investigation, we have varied ZnO concentration in the GO matrix to observe the field effect transport of the carriers and to understand the percolation threshold. The ZnO nanostructures anchored on GO surface modify the structure of GO and consequently changes the density of electrons and

Received: July 10, 2014
Accepted: September 9, 2014
Published: September 9, 2014

 © 2014 American Chemical Society  dx.doi.org/10.1021/am504501n | ACS Appl. Mater. Interfaces 2014, 6, 16941–16948

holes in the composite. Therefore, the field effect electrical characteristics of GO with gradual increase in ZnO concentration need to be studied for better understanding of charge transport phenomenon in the field effect regime. With the observations made from the transfer characteristics of FETs, made by the nanocomposites as channel layer, we have investigated how the conductivity is induced, the effect of ZnO concentration to tune the conductivity of GO, the transition from insulating to different conducting regimes under field effect transport and its origin.

## 2. EXPERIMENTAL WORK

**2.1. Synthesis of Graphene Oxide.** Graphene oxide was synthesized by a widely reported Hummer's method.[16] Briefly, graphite flakes (3 g) were oxidized using strong oxidizing agents such as $NaNO_3$ (1.5 g) and $KaMnO_4$(9 g) in $H_2SO_4$(69 mL). After oxidation, the mixture was washed until it attained a neutral pH value and was then dried at 55 °C for 8 h in a vacuum to obtain graphite oxide flakes.

**2.2. Synthesis of ZnO Nanostructures.** The ZnO nanostructures were prepared by a hydrothermal method.[17] Zinc acetate dehydrate (Zn $(CH3COO)_2{\cdot}2H_2O$, 2.195 g, Sigma-Aldrich) was ground in an agate mortar for 10 min. Ethanolamine (1 mL) was added to Zn $(CH3COO)_2{\cdot}2H_2O$ and ground for another 10 min and left for 2 h. Potassium hydroxide (0.6 g) was added to the mixture and ground for 1 h. The powder was washed in an ultrasonic bath repeatedly with water and alcohol. The product was dried in a vacuum at 80 °C for 2 h.

**2.3. Preparation of GO−ZnO Composite.** Graphite oxide flakes and ZnO nanostructures are dispersed separately in ethylene glycol with a concentration of 1 mg/mL. Four sets of GO−ZnO composites are made by mixing GO and ZnO dispersions, viz. (i) composite 1 [GO (95 wt %)- ZnO (5 wt %)], (ii) composite 2 [GO (90 wt %)−ZnO (10 wt %)], (iii) composite 3 [GO (85 wt %)−ZnO (15 wt %)], (iv) composite 4 [GO (80 wt %)− ZnO (20 wt %)] and (v) composite 5 [GO (75 wt %)−ZnO (25 wt %)]. After the solutions are mixed, the resultant dispersions are stirred for 12 h, for incorporating ZnO nanostructures homogeneously onto the GO matrix. The GO−ZnO composites are stirred for another 3 h under UV illumination (with a 110 mW/cm$^2$ mercury lamp, $\lambda$ = 350 nm) to support photocatalytic reduction. The GO−ZnO dispersions turn from brown to a black color, indicating the reduction of GO by ZnO nanostructures. The details of reduction mechanism are given elsewhere.[17,18]

**2.4. Fabrication of Thin-Film Transistors.** Field effect transistors with pristine GO and GO−ZnO composite as channel material are fabricated onto $SiO_2$/Si substrates (of dimension 3 × 3 cm) of oxide thickness 300 nm in a back gated configuration. The carrier concentration of Si is ~6.7 × $10^{16}$ cm$^{-3}$. Source and drain (Au) contacts of channel length 40 $\mu$m and width 500 $\mu$m are made by DC sputtering. Twenty such source-drain contacts were made. Field effect transistors were fabricated on drop casting the GO and composites onto each pair of the source and drain followed by annealing at 130 °C for 1 h in argon ambient, so that no two transistors interfere with each other. Figure 1 shows the schematic representation of FETs with GO−ZnO nanocomposite as the channel layer. The transfer and output characteristics were measured with a Keithley 4200 SCS semiconductor parameter analyzer under dark conditions.

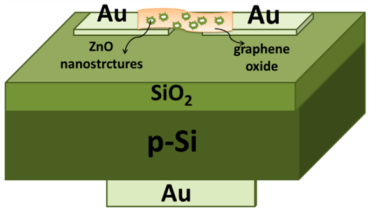


**Figure 1.** Schematic of GO−ZnO field effect transistors of channel length 40 $\mu$m and width 500 $\mu$m.

## 3. RESULTS AND DISCUSSION

The morphology of GO and its composites was observed using high resolution transmission electron microscopy (HRTEM). Figure 2a shows the HRTEM image of pristine GO. The ripples and wrinkles on the surface and paper like structure of pristine GO indicate its single or few layer characteristics. Figure 2b,c,d,e,f shows, respectively, the HRTEM images of composites 1−5. The white dots shown in the circle are the ZnO nanostructures on the GO matrix. From Figure 2b−f, it was observed that the ZnO nanostructures are uniformly dispersed and embedded onto the GO support. The increase in the concentration of ZnO nanostructures with increase in ZnO weight percentage from 5 to 25 wt % is clearly observed in HRTEM images from Figure 2b−f. The average size of the ZnO nanostructures is found to be in the range of 100 to 150 nm. The coverage area of ZnO on the GO surface increases with ZnO concentration; therefore, the oxygen functional groups on the surface of GO would be removed due to increase in ZnO weight percentage. As a result, the sp$^2$ electron network on GO surface would be restored.

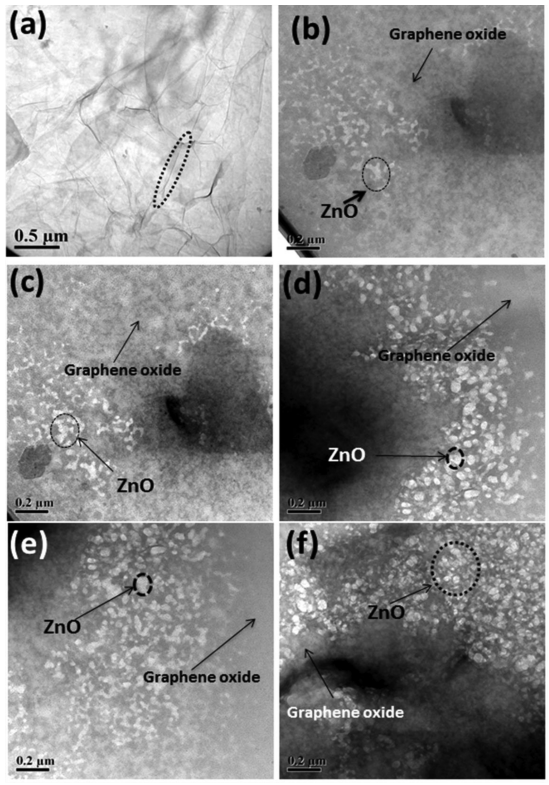


**Figure 2.** HRTEM image of (a) pristine GO, the wrinkles on the surface (encircled) showing single layer characteristics, GO−ZnO composite with ZnO (b) 5, (c) 10, (d) 15, (e) 20 and (f) 25 wt %.

Raman spectroscopy is a powerful and nondestructive technique to extract useful information about graphene and its related materials.[19,20] A monochromatic laser source is used that interacts with the molecular vibrational modes and phonons of graphene based materials. As a result, shifting in laser energy either down (stokes) or up (antistoke) is observed due to inelastic scattering between incident photons (from

laser) and phonons in graphene.[21] Therefore, two main peaks, G and D, are observed in graphene and its related materials. In pristine graphite, the G band is due to in-phase vibrations of the graphite lattice and D band arises due to disorder at graphite edges.[22]

The pristine GO and composite 5 (GO with 25 wt % ZnO) are characterized with 532 nm excitation laser and the corresponding Raman spectra is shown in Figure 3. In pristine

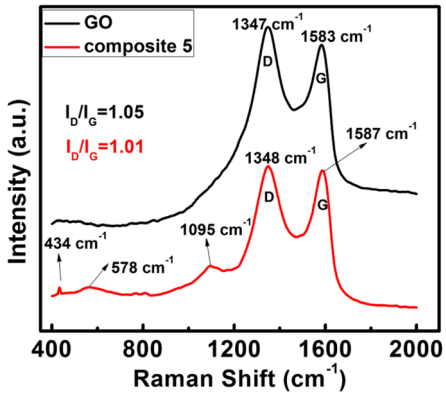


**Figure 3.** Raman spectra of pristine GO (black line) and composite 5 (red line). The intensity of D peak with respect to G peak is found to reduce in composite 5 compared to pristine GO due to anchoring of ZnO nanostructures.

GO (black line in Figure 3), the G and D bands are observed at Raman shifts of 1583 and 1347 $cm^{-1}$, respectively, with an intensity ratio, $I_D/I_G$ = 1.10. However, in the case of composite 5 (red line), the G and D bands are found to be at 1587 and 1348 $cm^{-1}$ with additional peaks at 434, 578 and 1095 $cm^{-1}$, which are due to ZnO nanostructures anchored onto the GO surface. These results are consistent with earlier reports on Raman spectra of GO and graphene oxide−ZnO composites.[23−27] The $I_D/I_G$ ratio in Raman spectra of composite 5 is found to be 1.01. The decrease in intensity of the D peak with respect to the G peak, i.e., decrease in $I_D/I_G$ ratio (1.01) in composite 5 compared to pristine GO ($I_D/I_G$ is 1.10) indicates the restoration of the $sp^2$ network on the surface of GO due to its photocatalytic reduction with ZnO nanostructures. The characteristic peak at 434 $cm^{-1}$ belongs to $E_2^{high}$ mode of vibrations in ZnO, indicating the wurtzite crystal phase of attached ZnO nanostructures.[28] The peak at 578 $cm^{-1}$ is the $E_1^{low}$ mode of vibrations corresponding to the oxygen deficiency defect in ZnO. The peak at 1095 $cm^{-1}$ is due to multiple phonon scattering processes in ZnO.[26]

Therefore, from Raman spectra, we have observed that the attachment of ZnO onto the GO matrix leads to partial restoration of the $sp^2$ network on the graphene basal plane in GO and attached ZnO nanostructures are in a wurtzite crystal structure.

Figure 4a shows the UV−visible spectra of GO and its composites, to observe the degree of oxidation in GO and its composites. These measurements are carried out by dispersing GO and its composites in ethylene glycol after a photocatalytic reduction reaction. In pristine GO (black line), the peak observed at 229 nm corresponds to $\pi \rightarrow \pi^*$ transition for C═C, which is consistent with the values reported earlier.[29] The maximum absorbance is observed at the lower wavelength range (227−231 nm), which is a characteristic of retaining more aromating rings on the GO surface due to oxidation.[30] Another small peak observed closer to 300 nm is due to the $n \rightarrow \pi^*$ transition of the carbonyl functional group. The intensity of the C═C peak would be higher for a more oxidized GO because the high degree of oxidation yields a greater amount of aromatic rings, which reflects the intensity of the C═C peak. Therefore, the ratio of the intensity of the peaks at 229 nm (i.e., C═C) and at ∼300 nm (due to carbonyl group) represents the degree of oxidation of GO.[31] In the present case, because the ratio is very high, it indicates a high degree of oxidation in pristine GO. However, the intensity of the C═C peak was found to be gradually reduced in GO composites (composites 1, 3 and 5) with increases in ZnO concentration, indicating the removal of oxygen functional groups due to a photocatalytic reduction reaction.

Because GO is a direct band gap semiconductor,[32] the band gap of pristine GO and its composites 1, 3 and 5 was obtained, as shown in Figure 4b. For further information on obtaining band gap using UV−visible spectra, one can refer the work carried out by Jeong et al.[33] and Shen et al.[34] on the synthesis and measurement of the band gap of GO with different degrees of oxidation. In Figure 4b, $A$ is the absorption coefficient of UV−visible light by GO and its composites, $h$ is the Planck's constant and $\nu$ is the frequency of UV−visible light. The band gaps of pristine GO and composites 1, 3 and 5 are found to be respectively, 3.98, 3.65, 3.21 and 2.8 eV. The band gap of GO is a function of its degree of oxidation, i.e., the amount of oxygen functional groups attached on the graphene basal plane.[35] Therefore, the band gap of pristine GO is high (3.98 eV) compared to those of its composites due to its high degree of

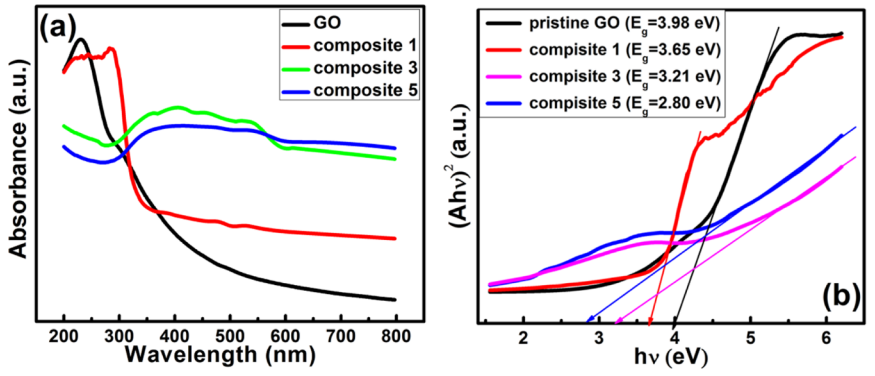


**Figure 4.** (a) UV−visible spectra and (b) band gap of GO, composites 1, 3 and 5. The band gap in pristine GO is 3.98 eV; however, the band gap decreases due to removal of oxygen groups on GO surface after the attachment of ZnO nanostructures.

oxidation. However, the band gap of the composite was found to decrease with increases in ZnO concentration due to removal of oxygen functional groups, which was also observed in the Raman spectra of GO and its composites (Figure 3).

The C 1s X-ray photoelectron spectroscopy (XPS) spectra of pristine GO and composites 1, 2, 3, 4 and 5 are shown, respectively, in Figure 5a,b,c,d,e,f. The signals were deconvoluted using a Gaussian−Lorentzian peak shape. The peaks at 284.5, 285.7 and 286.8 eV are, respectively, attributed to C—C (or C═C, C—H), C—OH (C—O—C) and C═O oxygen functional groups.[36,37] Figure 5a shows the XPS spectra of pristine GO in which the intensity of C−OH is nearly the same as that of the C═C peak, indicating a higher degree of oxidation of GO. It is observed from Figure 5b−f that the intensity of the C—OH group decreases with increases in ZnO loading from 5 to 25 wt %. As the ZnO nanostructures have affinity for C−OH functional groups, the intensity of C—OH functional group decreases with ZnO loading. Briefly, in the photoreduction of GO using ZnO nanostructures, the electrons generated from the electron−hole pair transferred to epoxide or hydroxyl functional groups (C—OH). As a result, the C—OH groups diminish with photoreduction, forming the $sp^2$ domains or islands (also observed from HRTEM, Raman and UV−visible spectra); hence the conductivity of GO−ZnO composite increases.

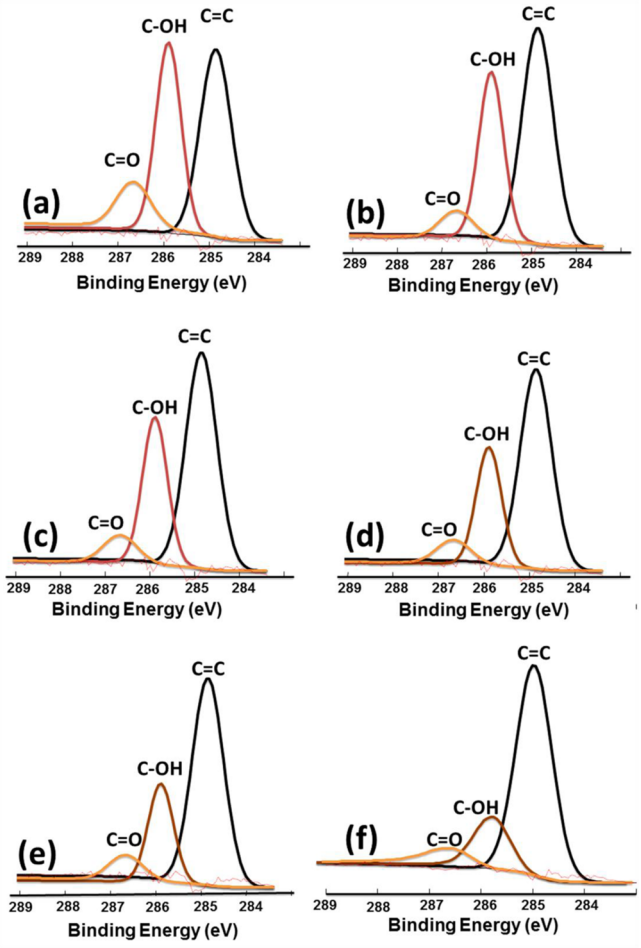


**Figure 5.** Panels a, b, c, d, e and f show XPS spectra of pristine GO and composites 1, 2, 3, 4 and 5, respectively.

The mechanism for the gradual reduction of GO by ZnO in ethanol is clearly explained by Akhavan;[38,39] one can refer these publications for better understanding of the photocatalytic reduction reaction. The photocatalytic reduction mechanism in GO due to anchoring of ZnO nanostructures in ethylene glycol is given by[40]

$$\mathrm{ZnO} + h\nu \rightarrow \mathrm{ZnO}(e^- + h^+) \quad (1)$$

$$\mathrm{ZnO}(e^- + h^+) \xrightarrow{C_2H_5OH} \mathrm{ZnO}(e^-) + C_2H_4OH \quad (2)$$

$$\mathrm{ZnO}(e^-) + \mathrm{GO} \rightarrow \mathrm{ZnO} + \mathrm{RGO} \quad (3)$$

When GO−ZnO composites are irradiated with an UV light source, the electrons in ZnO (with band gap 3.37 eV) are transferred from the valence band to the conduction band, resulting in the creation of electron−hole pairs. The photo generated holes create ethoxy radicals in ethylene glycol and the electrons are trapped by oxygen functional groups. Therefore, the oxygen groups are removed from the surface of GO leading to its reduction and restoration of $sp^2$ electron network. Thus, decrease in intensity of oxygen functional groups was observed in XPS spectra (Figure 5).

Figure 6a,b,c,d,e,f shows the transfer ($I_d - V_g$) characteristics of the devices (FET) made of pristine GO and composites 1, 2, 3, 4 and 5, respectively, at a drain-source voltage ($V_{ds}$) of 1 V. The corresponding output characteristics at different gate

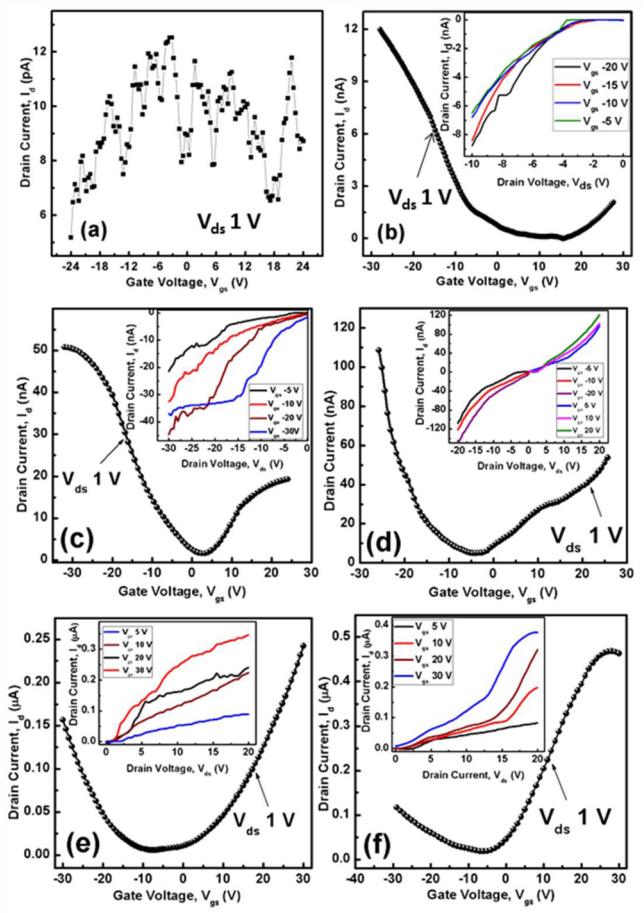


**Figure 6.** Transfer and output (inset) characteristics of FETs made of (a) pristine GO, (b) composite 1, (c) composite 2, (d) composite 3, (e) composite 4 and (f) composite 5 as channel layer.


dx.doi.org/10.1021/am504501n | ACS Appl. Mater. Interfaces 2014, 6, 16941−16948

voltages are shown in the inset. The drain current (shown in Figure 6a) was very low, on the order of pico ampere, in transistors with pristine GO as the channel layer due to its insulating characteristics. Figure 6b shows the improved transfer characteristics of GO with 5 wt % of ZnO loading (composite 1). Here it is observed that the transfer characteristics show *p*-type dominant electrical conductivity. Though the device exhibited *p*-type dominant conductivity, the current due to electrons (*n*-type) was significantly increased in composite 2 as the channel layer in the transistors (Figure 6c). This is due to an increase in ZnO loading from 5 to 10 wt %. The transfer characteristics of transistors with composite 3 as the channel layer showed nearly ambipolar characteristics (Figure 6d). However, *n*-type dominant characteristics were observed for composites 4 and 5, as shown in Figure 6e,f, respectively, indicating that the transition from *p*-type to *n*-type dominant conductivity in GO−ZnO composites occurred for ZnO concentrations between 15 and 20 wt %.

The output characteristics of GO−ZnO composites at various gate voltages are shown in the inset of the respective panels in Figure 6b−f and the drain current is found to be enhanced with the gate voltage. We have observed that the drain current increases abnormally after a certain initial drain-source voltage ($V_{ds}$) due to space charge limited conduction resulting in injection of charge carriers.[41]

The field effect mobility of the devices made of different ZnO loading is shown in Table 1. Both the electron and hole field effect mobility ($\mu_{FE}$) increase with ZnO loading. From Raman (Figure 3), UV−visible (Figure 4) and XPS spectra (Figure 5), we have observed the reduction of GO with ZnO causes removal of oxygen functional groups from GO surface. Therefore, the charge carriers can move easily in the GO matrix, hence the mobility of charge carriers is increasing. The highest electron field effect mobility, $\mu_{FE}$ is found to be 6.325 $cm^2/(V\ s)$ for the device made of composite 5. For the same composition, earlier, we obtained an electron $\mu_{FE}$ of 1.94 $cm^2/(V\ s)$.[15] The enhancement in mobility for the same composition of GO and ZnO (composite 5) is due to a decrease in channel length from 300 $\mu$m (in earlier work) to 40 $\mu$m (in the present work). Kobayashi et al.[42] reported that the field effect mobility of rGO sheets depends on channel length of the transistor. The reason is explained as follows. The lateral size of single GO sheet varies from 1 to 10 $\mu$m, depending on the preparation of GO sheets. Because we are dealing with multiple GO sheets decorated with ZnO, the 300 $\mu$m channel length consists of several GO sheets coupled together. This coupling increases the resistance between the adjacent GO nanosheets. Therefore, for a higher channel length, the inter sheet resistance between GO nanosheets increases, as a result the field effect mobility of charge carriers decreases. The contact resistance between adjacent GO sheets is low for the 40 $\mu$m channel length compared to that for the 300 $\mu$m channel. Therefore, the field effect mobility of charge carriers is found to be high in the present investigation for the 40 $\mu$m channel length compared to that for the 300 $\mu$m channel.[43]

**Table 1. Field Effect Mobility of GO−ZnO Composites**

| FETs made of | electron field-effect mobility $\mu_e$ $(cm^2/(V\ s))$ at $V_{ds}$ 1 V | hole field-effect mobility $\mu_h$ $(cm^2/(V\ s))$ at $V_{ds}$ 1 V |
|---|---|---|
| composite 1 | 0.760 | 1.124 |
| composite 2 | 1.675 | 2.325 |
| composite 3 | 3.350 | 3.425 |
| composite 4 | 4.850 | 4.530 |
| composite 4 | 6.325 | 5.900 |

In GO−ZnO composites, the *p*-type conductivity is due to the moisture and oxygen groups and the *n*-type conductivity is due to the $sp^2$ electrons in GO islands and ZnO nanostructures (being *n*-type). Initially, for composite 1, most of the oxygen groups are not reduced (from UV−visible (Figure 4) and XPS spectra, Figure 5b) and transport through these groups is dominant compared to electron flow through ZnO nanostructures. When more ZnO is loaded into the GO matrix, the oxygen groups are also reduced with the partial restoration of the GO surface (supported by data in Figures 2, 3, 4 and 5) and the concentration of free electrons increases. Therefore, the *n*-type dominant electron conductivity increases with the concentration of ZnO. Further, the dominant type of conductivity shifts from *p*-type to *n*-type. The electron affinity of graphene is −4.4 eV and that of ZnO is −4.3 eV.[14] Therefore, the transfer of electrons from ZnO nanostructures to graphene takes place easily by applying an external bias. From current−voltage characteristics, it is observed that as the concentration of ZnO increases in the GO−ZnO composite, the electrical conductivity of GO−ZnO composites also increases.

Figure 7 shows the field effect conductance (at $V_{ds}$ 1 V) of the transistors with composite 1 (Figure 7a) and composite 5 (Figure 7b) as the channel layer as a function of temperature in the range 150 to 300 K in steps of 50 K. We found that the field effect conductivity of composites increases with temperature, indicating semiconducting characteristics of GO−ZnO composites. Also, at low temperatures, we have observed stable *p*-type and *n*-type field effect conductivities, respectively, in composites 1 and 5.

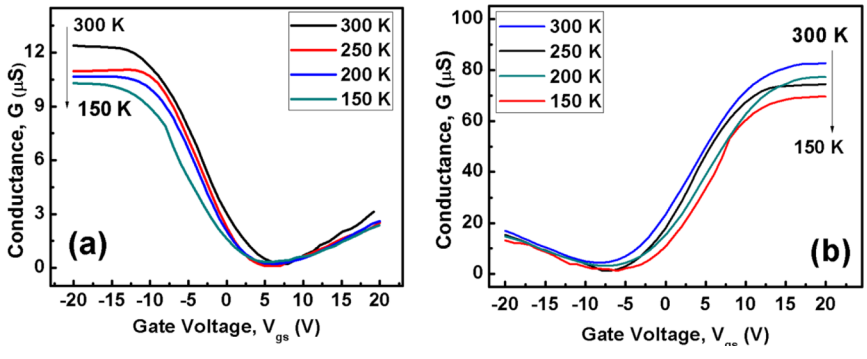


**Figure 7.** Temperature dependent transfer characteristics of transistors made with (a) composite 1 and (b) composite 5 as channel layer.

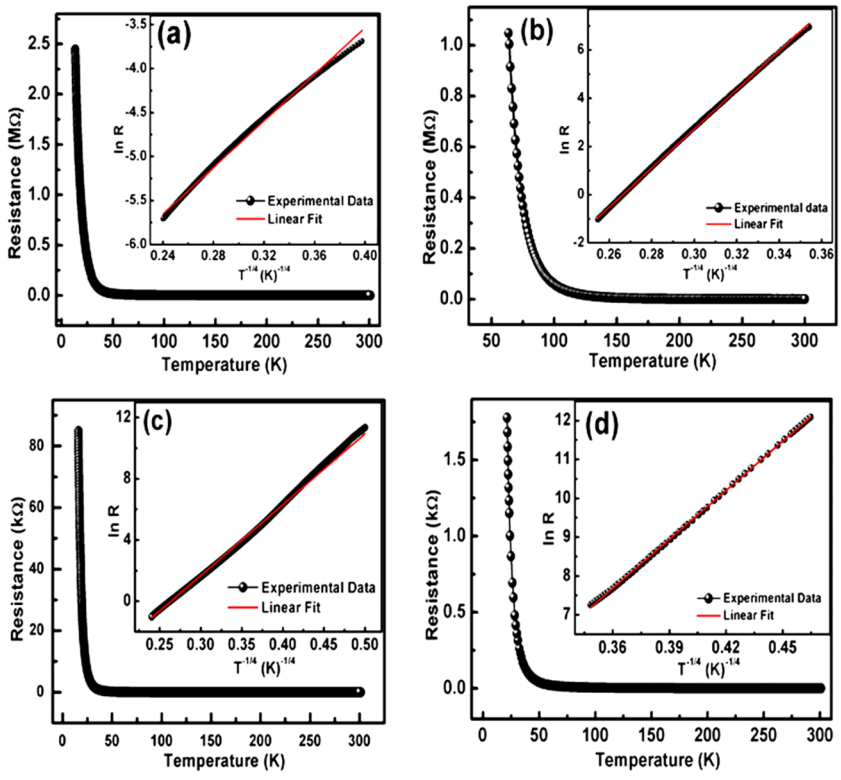


**Figure 8.** Temperature dependent resistance characteristics of (a) pristine GO, (b) composite 1, (c) composite 3 and (d) composite 5 with corresponding ln $R$ v/s $T^{-1/4}$ plot in the insets.

To study the charge transport in GO and GO−ZnO composites, the resistance of the samples was measured in the temperature range from 40 to 300 K. Figure 8a−d, respectively, shows the resistance of pristine GO and composites 1, 3 and 5 plotted as a function of temperature. The value of the resistance of GO and GO−ZnO composites is found to decrease exponentially with the temperature, indicating semiconducting characteristics of the samples. The temperature dependent resistance of GO and GO−ZnO composites was found to be linear when ln $R$ is plotted as a function of $T^{-1/4}$ (as shown in the inset of Figure 8a−d).

The charge transport in GO and GO−ZnO composites is observed to follow variable range hopping model, which describes the successive inelastic tunnelling between two localized states. The process, in general, is represented by the relation[43,44]

$$I = I_0 \exp\left[\left(\frac{-T_0}{T}\right)^{1/n}\right] \quad (4)$$

where $(n-1)$ is the dimensionality of the material.

The temperature dependent resistance data was fitted with different values of $n$ (2, 3, 4) and a linear plot was found for ln $R$ versus $T^{-1/4}$ (for $n = 4$), as shown in Figure 6 where $R$ is the resistance of GO and its composite thin film. Therefore, charge transport in multilayer both GO and GO−ZnO composites followthe Mott variable-range hopping mechanism.

## 4. CONCLUSION

In summary, we have studied the field effect electrical properties of GO−ZnO composites with different ZnO loading. From the transfer characteristics of the FETs, made of different composites, it is observed that the conductivity of GO−ZnO composites increases with the amount of ZnO loading. Initially, with a low amount of (5 wt %) ZnO, the devices showed $p$-type dominant electrical characteristics. With increases in the concentration of ZnO, enhancement in $n$-type conductivity is observed. Further, the field effect mobility of charge carriers also increases with the increase in the amount of ZnO. Thus, from the present investigation, it is observed that the electrical conductivity in GO is tuned from insulator to $p$-type to $n$-type with increase in ZnO loading. This behavior is attributed to the oxygen functional groups on GO sheets, which is found to reduce due to increase in the loading of ZnO nanostructures as in confirmed by the Raman, UV−visible and XPS measurements. The charge conduction in GO and GO−ZnO composites was found to follow the Mott variable-range hopping mechanism.

## AUTHOR INFORMATION

### Corresponding Author

*P. Banerji. E-mail: pallab@matsc.iitkgp.ernet.in. Phone: +91-3222-283984.

### Notes

The authors declare no competing financial interest.

## ACKNOWLEDGMENTS

One of the authors, Mr. S. Mahaboob Jilani, acknowledges the UGC-Maulana Azad National Fellowship for providing financial support. The authors also acknowledge the DST-FIST funded XPS facility at the Department of Physics and Meteorology, Indian Institute of Technology, Kharagpur, India.

## REFERENCES


(1) Eda, G.; Mattevi, C.; Yamaguchi, H.; Kim, H. K.; Chhowallah, M. Insulator to Semimetal Transition in Graphene Oxide. *J. Phys. Chem. C* **2009**, *113*, 15768−15771.

(2) Marcano, D. C.; Kosynkin, D. V.; Berlin, J. M.; Sinitskii, A.; Sun, Z.; Slesarev, A.; Alemany, L. B.; Lu, W.; Tou, J. M. Improved Synthesis of Graphene Oxide. *ACS Nano* **2010**, *4*, 4806−4814.

(3) Jung, I.; Dikin, D. A.; Piner, R. D.; Rouff, R. S. Tunable Electrical Conductivity of Individual Graphene Oxide Sheets Reduced at "Low" Temperatures. *Nano Lett.* **2008**, *8*, 4283−4287.

(4) Gilje, S.; Han, S.; Wang, M.; Wang, K. L.; Kaner, R. B. A Chemical Route to Graphene for Device Applications. *Nano Lett.* **2007**, *7*, 3394−3398.

(5) Zhu, H.; Ji, D.; Jiang, L.; Dong, H.; Hu, W. Tuning Electrical Properties of Graphite Oxide by Plasma. *Philos. Trans. R. Soc., A* **2013**, *371*, 20120308.

(6) Williams, G.; Kamat, P. V. Graphene−Semiconductor Nanocomposites: Excited-State Interactions between ZnO Nanoparticles and Graphene Oxide. *Langmuir* **2009**, *25*, 13869−13873.

(7) Zhuang, S.; Xu, X.; Feng, B.; Hu, J.; Pang, Y.; Zhou, G.; Tong, L.; Zhou, Y. Photogenerated Carriers Transfer in Dye-Graphene-$SnO_2$ Composites for Highly Efficient Visible-Light Photocatalysis. *ACS Appl. Mater. Interfaces* **2014**, *6*, 613−621.

(8) Joung, D.; Chunder, A.; Zhai, L.; Khondaker, S. I. High Yield Fabrication of Chemically Reduced Graphene Oxide Field Effect Transistors by Dielectrophoresis. *Nanotechnology* **2010**, *21*, 165202.

(9) Chen, J. H.; Jang, C.; Adam, S.; Fuhrer, M. S.; Williams, E. D.; Ishigami, M. Charged-Impurity Scattering in Graphene. *Nat. Phys.* **2008**, *4*, 377−381.

(10) McCreary, K. M.; Pi, K.; Swartz, A. G.; Han, W.; Bao, W.; Lau, C. N.; Guinea, F.; Katsnelson, M. I.; Kawakami, R. K. Effect of Cluster Formation on Graphene Mobility. *Phys. Rev. B* **2010**, *81*, 115453.

(11) McCreary, K. M.; Pi, K.; Kawakami, R. K. Metallic and Insulating Adsorbates on Grapheme. *Appl. Phys. Lett.* **2011**, *98*, 192101.

(12) Joung, D.; Singh, V.; Park, S.; Schulte, A.; Seal, S.; Khondaker, S. I. Anchoring Ceria Nanoparticles on Reduced Graphene Oxide and their Electrical Transport. *J. Phys. Chem. C* **2011**, *115*, 24494−24500.

(13) Wang, W.; Lian, J.; Cui, P.; Xu, Y.; Seo, S.; Lee, J.; Chan, Y.; Lee, H. Dual n-Type Doped Reduced Graphene Oxide field Effect Transistors Controlled by Semiconductor Nanocrystals. *Chem. Commun.* **2012**, *48*, 4052−4054.

(14) Yoo, H.; Kim, Y.; Lee, J.; Lee, H.; Yoon, Y.; Kim, G.; Lee, H. n-Type Reduced Graphene Oxide Field-Effect Transistors (FETs) from Photoactive Metal Oxides. *Chem.—Eur. J.* **2012**, *18*, 4923−4929.

(15) Jilani, S. M.; Gamot, T. D.; Banerji, P. Thin Film Transistors with Graphene Oxide Nanocomposite Channel. *Langmuir* **2012**, *28*, 16485−16489.

(16) Hummers, W. S.; Offeman, R. E. Preparation of Graphitic Oxide. *J. Am. Chem. Soc.* **1958**, *80*, 1339−1339.

(17) Jin, C. F.; Yuan, X.; Ge, W. W.; Hong, J. M.; Xin, X. Q. Synthesis of ZnO Nanorods by Solid State Reaction at Room Temperature. *Nanotechnology* **2003**, *14*, 667.

(18) Willium, G.; Kamat, P. V. Graphene-Semiconductor Nanocomposites: Excited-State Interactions between ZnO Nanoparticles and Graphene Oxide. *Langmuir* **2009**, *25*, 13869−13873.

(19) Wei, Z.; Wang, D.; Kim, S.; Kim, S. Y.; Hu, Y.; Yakes, M. K.; Laracuente, A. R.; Dai, Z.; Marder, S. R.; Berger, C.; King, W. P.; de Heer, W. A.; Sheehan, P. E.; Riedo, E. Nanoscale Tunable Reduction of Graphene Oxide for Graphene Electronics. *Science* **2010**, *328*, 1073−1076.

(20) Cheng, M.; Yang, R.; Zhang, L.; Shi, Z.; Yang, W.; Wang, D.; Xie, G.; Shi, D.; Zhang, G. Restoration of Graphene from Graphene Oxide by Defect Repair. *Carbon* **2012**, *50*, 2581−2587.

(21) Yanga, D.; Velamakannia, A.; Bozoklub, G.; Parka, S.; Stollera, M.; Pinera, R. D.; Stankovichc, S.; Junga, I.; Field, D. A.; Ventrice, C. A., Jr.; Ruoff, R. S. Chemical Analysis of Graphene Oxide films after Heat and Chemical Treatments by X-Ray Photoelectron and Micro-Raman Spectroscopy. *Carbon* **2009**, *47*, 147−152.

(22) Ferrari, A. C.; Meyer, J. C.; Scardaci, V.; Casiraghi, C.; Lazzeri, M.; Mauri, F.; Piscanec, S.; Jiang, D.; Novoselov, K. S.; Roth, S.; Geim, A. K. Raman Spectrum of Graphene and Graphene Layers. *Phys. Rev. Lett.* **2006**, *97*, 187401.

(23) Yin, Z.; Wu, S.; Zhou, X.; Huang, X.; Zhang, Q.; Boey, F.; Zhang, H. Electrochemical Deposition of ZnO Nanorods on Transparent Reduced Graphene Oxide Electrodes for Hybrid Solar Cells. *Small* **2010**, *6*, 307−312.

(24) Luo, Q. P.; Yu, X. Y.; Lei, B. X.; Chen, H. Y.; Kuang, D. B.; Su, C. Y. Reduced Graphene Oxide-Hierarchical ZnO Hollow Sphere Composites with Enhanced Photocurrent and Photocatalytic Activity. *J. Phys. Chem. C* **2012**, *116*, 8111−8117.

(25) Ha, T. J.; Lee, J.; Chowdhury, S. F.; Akinwande, D.; Rossky, P. J.; Dodabalapur, A. Transformation of the Electrical Characteristics of Graphene Field-Effect Transistors with Fluoropolymer. *ACS Appl. Mater. Interfaces* **2013**, *5*, 16−20.

(26) Zhan, Z.; Zheng, L.; Pan, Y.; Sun, G.; Li, L. Self-Powered, Visible-Light Photodetector Based on Thermally Reduced Graphene Oxide−ZnO (rGO−ZnO) Hybrid Nanostructure. *J. Mater. Chem.* **2012**, *22*, 2589−2595.

(27) Liu, Y.; Hu, Y.; Zhou, M.; Qian, H.; Hu, X. Microwave-Assisted Non-Aqueous Route to Deposit Well-Dispersed ZnO Nanocrystals on Reduced Graphene Oxide Sheets with Improved Photoactivity for the Decolorization of Dyes Under Visible Light. *Appl. Catal., B* **2012**, *125*, 425−431.

(28) Xiao, Z.; Liu, Y.; Zhang, J.; Zhao, D.; Lu, Y.; Shen, D.; Fan, X. Electrical and Structural Properties of p-Type ZnO:N Thin Films Prepared by Plasma Enhanced Chemical Vapour Deposition. *Semicond. Sci. Technol.* **2005**, *20*, 796−800.

(29) Paredes, J. I.; Rodil, S. V.; Alonso, A. M.; Tascón, J. M. D. Graphene Oxide Dispersions in Organic Solvents. *Langmuir* **2008**, *24*, 10560−10564.

(30) Li, D.; Muller, M. C.; Gilje, S.; Kaner, R. B.; Vallace, G. G. Processable Aqueous Dispersions of Graphene Nanosheets. *Nat. Nanotechnol.* **2008**, *3*, 101−105.

(31) Zhang, J.; Yang, H.; Shen, G.; Cheng, P.; Zhang, J.; Guo, S. Reduction of Graphene Oxide via L-Ascorbic Acid. *Chem. Commun.* **2009**, *46*, 1112−1114.

(32) Seo, H.; Ahn, S.; Kim, J.; Lee, Y. A.; Chung, K. H.; Jeon, K. J. Multi-Resistive Reduced Graphene Oxide Diode with Reversible Surface Electrochemical Reaction Induced Carrier Control. *Sci. Rep.* **2014**, *4*, 1−7.

(33) Jeong, H. K.; Jin, M. H.; So, K. P.; Lim, S. C.; Lee, Y. H. Tailoring the Characteristics of Graphite Oxides by Different Oxidation Times. *J. Phys. D: Appl. Phys.* **2009**, *42*, 065418.

(34) Shen, Y.; Yang, S.; Zhou, P.; Sun, Q.; Wang, P.; Wan, L.; Li, J.; Chen, L.; Wang, X.; Ding, S.; Zhang, D. W. Evolution of the Band-Gap and Optical Properties of Graphene Oxide with Controllable Reduction Level. *Carbon* **2013**, *62*, 157−164.

(35) Shao, G.; Lu, Y.; Wu, F.; Yang, C.; Zeng, F.; Wu, Q. Graphene Oxide: The Mechanisms of Oxidation and Exfoliation. *J. Mater. Sci.* **2012**, *47*, 4400−4409.

(36) Yang, Y.; Ren, L.; Zhang, C.; Huang, S.; Liu, T. Facile Fabrication of Functionalized Graphene Sheets (FGS)/ZnO Nanocomposites with Photocatalytic Property. *ACS Appl. Mater. Interfaces* **2011**, *3*, 2779−2785.

(37) Dreyer, D. R.; Park, S.; Bielawski, C. W.; Ruoff, R. S. The chemistry of Graphene Oxide. *Chem. Soc. Rev.* **2010**, *39*, 228−240.

(38) Akhavan, O. Photocatalytic Reduction of Graphene Oxides Hybridized by ZnO Nanoparticles in Ethanol. *Carbon* **2011**, *49*, 11−18.

(39) Akhavan, O. Graphene Nanomesh by ZnO Nanorod Photocatalysts. *ACS Nano* **2010**, *4*, 4174−4180.

(40) Sarkar, S.; Basak, D. The Reduction of Graphene Oxide by Zinc Powder to Produce a Zinc Oxide-Reduced Graphene Oxide Hybrid and its Superior Photocatalytic Activity. *Chem. Phys. Lett.* **2013**, *561*, 125−130.

(41) Prakash, A.; Bahadur, D. The Role Of Ionic Electrolytes on Capacitive Performance of ZnO-Reduced Graphene Oxide Nano-

hybrids with Thermally Tunable Morphologies. *ACS Appl. Mater. Interfaces* **2014**, *6*, 1394−1405.
(42) Kobayashi, T.; Kimura, N.; Chi, J.; Hirata, J.; Hobara, D. Channel-Length-Dependent Field-Effect Mobility and Carrier Concentration of Reduced Graphene Oxide Thin-Film Transistors. *Small* **2010**, *6*, 1210−1215.
(43) Jung, I.; Dikin, D. A.; Piner, R. D.; Rouff, R. S. Tunable Electrical Conductivity of Individual Graphene Oxide Sheets Reduced at "Low" Temperatures. *Nano Lett.* **2008**, *8*, 4283−4287.
(44) Venugopal, G.; Krishnamoorthy, K.; Mohan, R.; Kim, S. J. An Investigation of the Electrical Transport Properties of Graphene-Oxide Thin Films. *Mater. Chem. Phys.* **2012**, *132*, 29−33.